

# CONCEPT OF “FRACTAL” HELICOPTER TRIM PANEL

J eremie Derr  and Frank Simon

ONERA - The French Aerospace Lab, F-31055 Toulouse Cedex 4, France

E-mail addresses: jeremie.derre@onera.fr (J. Derr ), frank.simon@onera.fr (F. Simon).

The reduction of structural vibrations and acoustic radiation has become increasingly challenging due to mass reduction and the use of lightweight materials, especially in the aerospace industry. This paper presents the vibroacoustic behaviour of sandwich constructions locally overloaded by a pre-fractal mass distribution. The structural mechanical model consists in a homogenised beam in simple bending, approximated by finite differences and solved numerically to form a modal basis (eigenvalues and eigenvectors). The self-similar mass distribution, inspired from the Cantor set, is presented and integrated using local overloadings within the structure, which leads to a strong localisation of the beam transverse displacement. An analysis of the integrated density of states points out localised modes and their types (central or lateral localisation). Finally, acoustic coupling is modelled through a radiation resistance matrix from a discretisation of the structure into rectangular elementary radiators. Simulations exhibit a smaller radiation efficiency and lower modal critical frequencies. These results are encouraging for reducing the acoustic radiation of lightweight structures.

## NOMENCLATURE

$[\mathbb{I}_{N-1}]$	identity matrix of dimension $(N - 1)$	$h$	beam total thickness (m)
$[M]$	symmetric matrix	$h_c$	core thickness (m)
$[R]$	radiated resistance matrix	$h_s$	skin thickness (m)
$[Z]$	complex impedance matrix	$h_x$	segment length (m)
$\alpha_{loc}$	local overloading mass ratio	$I_c$	core second moment of area ( $m^4$ )
$\alpha_{tot}$	global overloading mass ratio	$I_s$	skin second moment of area ( $m^4$ )
$\mathbf{0}_{N-1}$	null vector of dimension $(N - 1)$	$L_x$	beam length (m)
$\mathbf{p}_e$	radiator element wall pressure	$L_y$	beam width (m)
$\mathbf{U}$	transverse displacement vector	$M_{over}$	local additional mass (kg)
$\mathbf{v}_e$	radiator element surface velocities	$N$	number of segments
$\omega$	angular frequency ( $rad.s^{-1}$ )	$n_{frac}$	pre-fractal order
$\rho$	homogenised material density ( $kg.m^{-3}$ )	$N_{rad}$	rectangular elementary radiator number
$\rho_0$	air density at NTP ( $kg.m^{-3}$ )	$p$	additional mass number
$\sigma$	acoustic radiation efficiency	$P_{ac}$	far-field total acoustic radiated sound power
$\sigma_m$	mode $m$ acoustic efficiency	$P_{vib}$	vibrational reference power
$c_0$	sound velocity in air at NTP ( $m.s^{-1}$ )	$S$	beam cross section ( $m^2$ )
$D$	approximate total bending stiffness ( $Pa.m^4$ )	$S_e$	elementary radiator surface ( $m^2$ )
$D_{sand}$	equivalent bending stiffness ( $Pa.m^4$ )	$u(x)$	beam transverse displacement (m)
$DOS$	density of states	$u(x_i)$	point $x_i$ displacement (m)
$E_c$	core Young's modulus (Pa)	$u_z(x, t)$	time dependant transverse displacement (m)
$E_s$	skin Young's modulus (Pa)	$v_n^2(\omega)$	normal averaged quadratic surface velocity
$FD$	finite difference	$x_i$	segment delimiting point

## 1 INTRODUCTION

In the aerospace industry, sandwich honeycomb core panels have been widely used for decades within secondary aircraft parts (*e.g.*, trim panels), because of

their high static bending stiffness at a lesser mass cost. The type of sandwich considered in this paper consists of two thin but sufficiently stiff laminates bonded to each side of a relatively thick and lightweight core. Nowadays, they are still of great interest and developments are

continuously made to reinforce them, in order to finally get them integrated as primary parts (NHIndustries NH90 for instance, fuselage or structural elements). The weight reduction is unfortunately responsible for a rise in the panel acoustic transmission over the critical frequency,<sup>[1]</sup> which has to be compensated.

In noise reduction, several strategies are based on the passive principle of structural vibration reduction to minimize the radiated noise. Damped viscoelastic material can be added onto the sandwich external skin, either covering all the panel surface or localised as small patches. Another technique used in the helicopter industry consists in filling out the honeycomb core with small elements such as empty spheres made of elastomer. Nonetheless, instead of reducing the global vibration amplitudes, the wave propagation in the vibrating material can be modified by introducing additional elements within the structure.

The additional elements (irregularities, heterogeneities or others) can be distributed within the initial structure, following a periodic,<sup>[2,3]</sup> random,<sup>[4]</sup> as well as self-similar patterns.<sup>[5,6,7]</sup> The structure itself can be composed of several sub-parts connected together to form a multi-span system.<sup>[8,9]</sup> In both cases, material and geometrical discontinuities create diffraction, reflection, transmission and even dissipation phenomena, which lead to the apparition of stop-bands and pass-bands in the frequency content, as well as a concentration of the mechanical energy and thus the localisation of the structure mode shapes. Therefore, the structure can be considered as a mechanical filter for wave propagation.

Recent studies have shown encouraging mechanical results on self-similar configurations such as string<sup>[6]</sup> and membrane.<sup>[7]</sup> Simulations identify localisation phenomena of the transverse displacement, confirmed by some experimental data. Integrated density of states are analysed, as well as the heterogeneity distribution role and the corresponding modification on modal shapes. The potential of such configurations motivates its application to the helicopter industry. Trim panels are responsible for the most part of radiated noise within the aircraft cabin. These panel surface areas are about a square meter.

The global aim is to reduce the generated sound of vibrating panels, in the frequency bands of interest (main gear box noise or aerodynamic excitation for instance).

In this paper, the key idea is to use the geometrical cell network of the honeycomb core, and to fill out some cells by following a self-similar scheme. Indeed, the transition between two media of different natures and densities (empty cell and cell fully filled of spheres) could be seen for a bending wave as a mechanical impedance discontinuity, leading to multiple scattering phenomena. Thus, the idea is to use the properties of the

full cell network to create localised modes, resulting of wave pseudo-stationarity between heterogeneities.

There are two main particularities to the present study. The first one is the application of the well-known theory of pre-fractal distribution to a composite material, *i.e.* a sandwich beam. The second one is that the loading is realized within the material core, meaning that the structure load-bearing capability is not altered, which is of primordial importance from a mechanical point of view. Sample panels have already been realized and characterized in transmission with promising results.<sup>[10]</sup> From an industrial point of view, the manufacturing of such panels has been carried out manually without any specific issues.

The paper is organized in five sections. Following the introduction, the developed mechanical model is first presented for a monodimensional homogenised structure in Section 2. In Section 3, the heterogeneity integration into the model is described. Then, the self-similar distribution inspired from the Cantor set is briefly introduced, followed by simulation results of a localised mode for several orders of the self-similar scheme. Section 4 analyses the integrated density of states, identifying localised and classical extended modes. The vibroacoustic behaviour is presented in Section 5, and modal acoustic radiation efficiency is simulated and discussed. Finally, the conclusion and potential extensions are summarized in Section 6.

## 2 MECHANICAL MODEL OF A HOMOGENISED BENDING BEAM

The first step is a presentation of the mechanical model of a non-overloaded sandwich structure governed by bending dynamics.

### 2.1 Composite homogenisation

A typical sandwich trim panel construction is a core material trapped between two laminate sheets of glass-fiber. Herein, the core is made of an aramid fibre paper impregnated with a heat resistant phenolic resin and arranged in honeycomb hexagonal cells. The purpose of such a core is to maintain distance between the laminates and to some extent, to resist shear deformation.<sup>[11]</sup>

In the modelling of acoustic radiation created by mechanical vibration (fluid-structure interaction), bending waves have a predominant role in the sound frequency domain.<sup>[12]</sup>

Under Nilsson assumptions<sup>[13]</sup> (homogeneity and isotropy of all layers and skins assumed thin), an equivalent bending stiffness of the whole structure can be derived using Huygens theorem. The resulting equivalent

bending stiffness  $D_{\text{sand}}$  is given by

$$\begin{aligned} D_{\text{sand}} &= E_c I_c + E_s I_s, \\ &= E_c \frac{L_y h_c^3}{12} + 2 E_s \left( \frac{L_y h_s^3}{12} + L_y h_s \left( \frac{h_c + h_s}{2} \right)^2 \right), \end{aligned} \quad (1)$$

where Young's modulus and second moment of area (of the cross section) of the core ( $c$ ) and of the skins ( $s$ ) are identified respectively by  $E$  and  $I$ , as well as thicknesses of elements  $h$  and the beam width is  $L_y$ .

Kim and Hwang<sup>[14]</sup> examined the validity conditions of the approximation used in such a model. Bending stiffness of the skins projected to the neutral line of the sandwich beam is predominant and thus, the approximate total bending stiffness could be written as

$$D = E_s L_y h_s \frac{(h_c + h_s)^2}{2}, \quad (2)$$

where the thickness ( $h_c + h_s$ ) confers the ensemble a large equivalent bending stiffness, called sandwich effect. In the following of the paper, the structure is considered as an homogeneous equivalent material, described with the previous Eq. (2).

Due to its complex constitution, the mechanical behaviour of a sandwich beam involves different parts of the structure depending on frequency. However, the global behaviour at high frequencies is governed by the bending dynamics of the laminates,<sup>[11]</sup> which gives consistency to our approach. Indeed, the strong localisation phenomena are expected for high mode orders. As long as the first model is a beam, the frequencies of interest would then be shifted towards to higher frequencies due to its small width.

## 2.2 Simple bending beam

Under the previous hypotheses and approximations, a fourth-order beam theory is used. Considering a straight slender Euler-Bernoulli beam, and time-dependency taken as harmonic with angular frequency  $\omega$ , the transverse displacement of the beam  $u_z(x, t) = u(x) \times \exp(j\omega t)$  is governed by equilibrium Eq. (3)

$$\frac{D}{\rho S} \frac{d^4 u(x)}{dx^4} - \omega^2 \cdot u(x) = 0, \quad (3)$$

with the cross section  $S = hL_y$  (total beam thickness by its width) and  $\rho$  the density of the material.

## 2.3 Discretisation

The choice of derivative approximation and structure discretisation by finite difference (abbreviated FD) method is mainly justified by its convenience and the flexibility of its implementation regarding the different orders of self-similar distributions which are integrated

within the structure.

Given a beam under the aforementioned hypothesis, of length  $L_x$ , the structure is divided into  $N$  segments of constant length  $h_x$  as  $L_x = h_x \times N$ . A set of  $(N + 1)$  points ( $x_i$ ) delimiting the segments is defined as  $x_i = (i - 1) \times h_x$ , with  $x_1$  and  $x_{N+1}$  the beam extremities. Finally, the transverse displacement at position  $x_i$  is written as  $u(x_i) = u_i$ .

Following the classical FD technique, such as Subrahmanyam and Leissa,<sup>[15]</sup> Eq. (3) is approximated with a second order central scheme, which gives the equilibrium around position  $x_i$  as

$$\frac{D}{\rho S h_x^4} \left[ u_{i-2} - 4u_{i-1} + 6u_i - 4u_{i+1} + u_{i+2} \right] - \omega^2 \cdot u_i = 0. \quad (4)$$

### 2.3.1 Boundary conditions

In this study, the beam is considered as simply supported in its width and free in its length. To integrate boundary conditions, a method based on the creation of off-domain supplementary points is used. These points are linked by FD relationships and substituted, then integrated to the equations of the physical domain.

### 2.3.2 Matrix notation

Once the boundary conditions are integrated, the following system (5) is obtained, with  $(N - 1)$  equations

$$\left\{ \begin{array}{l} (i = 2) : \frac{D}{h_x^4} [5u_2 - 4u_3 + u_4] - \omega_n^2 \rho S \cdot u_2 = 0, \\ (i = 3) : \frac{D}{h_x^4} [-4u_2 + 6u_3 - 4u_4 + u_5] - \omega_n^2 \rho S \cdot u_3 = 0, \\ \dots \\ (i) : \frac{D}{h_x^4} [u_{i-2} - 4u_{i-1} + 6u_i - 4u_{i+1} + u_{i+2}] - \omega_n^2 \rho S \cdot u_i = 0, \\ \dots \\ (i = N-1) : \frac{D}{h_x^4} [u_{N-3} - 4u_{N-2} + 6u_{N-1} - 4u_N] - \omega_n^2 \rho S \cdot u_{N-1} = 0, \\ (i = N) : \frac{D}{h_x^4} [u_{N-2} - 4u_{N-1} + 5u_N] - \omega_n^2 \rho S \cdot u_N = 0. \end{array} \right. \quad (5)$$

The  $\omega_n$  are discrete. Indeed, the system dimension is  $n$  and thus the number of degrees of freedom is fixed. The previous system can be rewritten as Eq. (6), where matrix  $[M]$  is a symmetric pentadiagonal matrix,  $[\mathbb{I}_{N-1}]$  is the identity matrix of dimension  $(N - 1)$ ,  $\mathbf{U}$  is the vector of transverse displacements and  $\mathbf{0}_{N-1}$  the null vector of  $(N - 1)$  components

$$\left\{ \left( \frac{D}{\rho S \cdot h_x^4} \right) [M] - \omega_n^2 [\mathbb{I}_{N-1}] \right\} \mathbf{U} = \mathbf{0}_{N-1}. \quad (6)$$

Eq. (6) is an eigenvalue problem, which is solved to form a modal basis of the structure (eigenvalues and eigenvectors for natural frequencies and mode shapes respectively).

### 3 MECHANICAL BEHAVIOUR OF A STRUCTURE LOADED BY A SELF-SIMILAR DISTRIBUTION

This part aims at describing how the heterogeneities are integrated within the structure and how they are modelled in the FD scheme. The self-similar distribution is then presented. Finally, the shape of a given localised mode is computed for different pre-fractal orders.

#### 3.1 Integration of heterogeneities following a pre-fractal scheme

The patent<sup>[10]</sup> presents the concept of elements distributed following a self-similar scheme in the core of composite sandwich panels. Preliminary experiments featured localisation phenomena and identified the added mass as the key element of overloaded structures.

##### 3.1.1 Integration of a single heterogeneity

Given that the main mechanism identified is mass adding, it is modelled as the local overload of a discrete element, and can represent a heterogeneity within the honeycomb core. As mentioned above, transition between two different media creates an impedance breakdown. Therefore, the addition of a small mass  $M_{\text{over}}$  on a discrete element  $k$  is modelled as in Eq. (7)

$$\frac{D}{h_x^3} \left[ u_{k-2} - 4u_{k-1} + 6u_k - 4u_{k+1} + u_{k+2} \right] - \omega_n^2 \left( \rho S + \frac{M_{\text{over}}}{h_x} \right) \cdot u_k = 0. \quad (7)$$

The local overloading mass ratio is defined as Eq. (8)

$$\alpha_{\text{loc}} = \frac{\rho S}{\left( \rho S + M_{\text{over}}/h_x \right)}, \quad (8)$$

leading to the following formulation

$$\alpha_{\text{loc}} \left( \frac{D}{\rho S h_x^3} \left[ u_{k-2} - 4u_{k-1} + 6u_k - 4u_{k+1} + u_{k+2} \right] \right) - \omega_n^2 \cdot u_k = 0, \quad (9)$$

which is the  $k$ -line of matrix  $[M]$  multiplied by  $\alpha_{\text{loc}}$  in Eq. (6).

##### 3.1.2 Self-similar scheme

The studied structure is the homogenised beam as described previously, overloaded by a self-similar distribution inspired by the Cantor set. This iterative construction process has an homothetic ratio of three: at each iteration (order), the element is sub-divided into three parts and the central one is removed. The first three orders of this motif are presented on Figure 1, as well as order 0, which is the initial structure. The distribution used is strongly inspired from this set, except that only the extremities of the sub-sets are marked and correspond to local overloadings. Is called fractal the

object obtained when a self-similar pattern construction is infinitely repeated, and this is why in the present case the motif is called pre-fractal with a finite iteration order  $n_{\text{frac}}$ .



Figure 1: Original Cantor set, orders 0 to 3.

Based on the construction structure,<sup>[6]</sup> a self-similar beam of pre-fractal order  $n_{\text{frac}}$  is overloaded by  $p$  masses with

$$p = \sum_{i=1}^{n_{\text{frac}}} 2^i = 2 \times (2^{n_{\text{frac}}} - 1). \quad (10)$$

##### 3.1.3 Integration of the pre-fractal distribution

For a given  $n_{\text{frac}}$  pre-fractal order,  $p$  local masses are integrated on the extremities of the sub-sets defined previously. This leads to multiplications of the  $p$  corresponding lines of matrix  $[M]$  by  $\alpha_{\text{loc}}$ .

It is noticeable that the discretisation in  $N$  segments plays a crucial role regarding the size of the discrete elements. Indeed, even though masses are taken as points, they stand for a segment of equivalent length  $h_x$ . The discretisation is therefore of primordial importance and a key feature in the model for simulations.

Figure 2 sketches simply-supported beams with the previously described Cantor-like set, from order 0 to 3. Overloaded masses are represented by black dots.

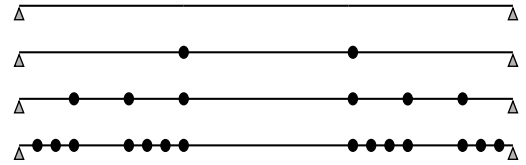


Figure 2: Self-similar loaded beam sketch, orders 0 to 3.

#### 3.2 Localisation of transverse displacement and mechanical behaviour

Figure 3 presents a simulation of shapes of mode 26 in the non-overloaded case and for beams overloaded by self-similar distribution at order 2 and 3, computed with a finite difference method, with  $N = 243$  segments. All quantities of the numerical simulations are summarised in Table 1 on the appendix. Mode identification and numbering corresponds to the number of transverse nodes, as for a classical homogeneous beam. In this paper, *classical* beam refers to a non-overloaded beam.

The global overloading mass ratio  $\alpha_{\text{tot}}$  of the beam is defined as the ratio of added overload masses on non-

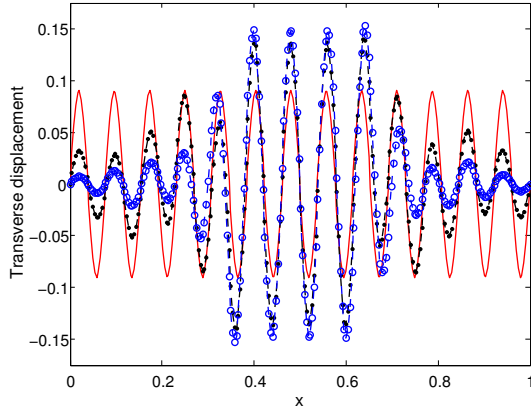


Figure 3: Transverse deflection (mode 26) : (—) classical beam (analytical), (---) pre-fractal beam of order 2 (FD) and (-o-) pre-fractal beam of order 3 (FD).

overloaded beam mass as

$$\alpha_{\text{tot}} = \frac{p \times M_{\text{over}}}{\rho L_x}. \quad (11)$$

Total beam overload ratio  $\alpha_{\text{tot}}$  is about 32% at order 2 and about 75% at order 3.

The mode shapes of Figure 3 are normalized by Euclidean norm equals to unity. The displacements of the central part have a significantly larger amplitude than those on lateral side parts. For the second-order structure, a localisation ratio (ratio between maximal amplitudes of the central part and of the lateral parts) close to three can be observed; for the third-order structure, it is about four. It can also be noted that the global behaviour of the curve does not present any singular point. Indeed, bending waves are not completely stopped at the heterogeneities but partially reflected and transmitted. The local overloading ratio  $\alpha_{\text{loc}}$  remains constant for the different orders presented and is about 0,071. In the case of a helicopter sandwich material, this corresponds to a core cell filled with a material of density about 3800 kg.m<sup>-3</sup>, which lies within the ceramic ranges.

#### 4 ROLE OF THE PRE-FRACTAL DISTRIBUTION ON INTEGRATED DENSITY OF STATES

The phenomenon of mode localisation can be clearly identified on integrated density of state (abbreviated DOS) curves, as illustrated on Figure 5.

Figure 4 is first analysed because plotted in logarithmic scale, which emphasises the phenomena representation. It presents the first set of *extended* and *localised* modes. An extended mode is a classical modal mode whose maxima stand at the same amplitude. Several areas of the DOS behaviours are identified, directly linked to the self-similar overloaded distribution:

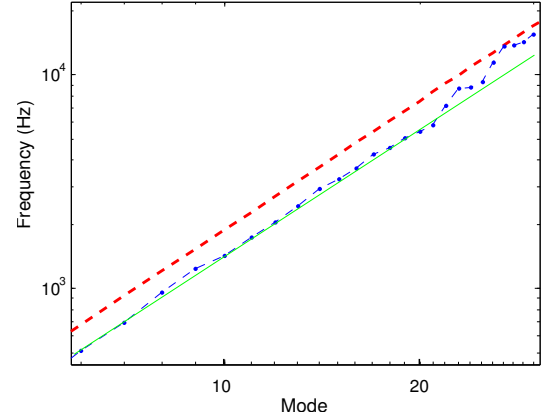


Figure 4: Natural frequencies of first 30 modes : (- -) classical beam, (- -) pre-fractal beam (order 3), and (—) homogeneous beam of equivalent mass of pre-fractal beam (log scales).

- In the low frequency region, the DOS curve of overloaded beam is quasi-identical to the classical beam, meaning a linear curve of constant slope (in logarithmic axis). The only impact of the overloading in these modes is a modification of the y-intercept. The fractal does not influence these modes, which are so-called *extended* modes. In the case of the order-three Cantor-like distribution, this corresponds to the first 20 modes.
- The first slope breakdown corresponds to the first modes with a localisation of the transverse displacement (mode 21 in the present study case), abbreviated localised modes. Indeed, these modes exhibit a mechanical energy concentration in the central part of the beam. For mode 22, central-to-lateral amplitude ratio is about three.
- The second slope breakdown appears at mode 23, for two modes localised on the non-overloaded lateral areas of the pre-fractal beam. These modes have a strong localisation ratio (more than 3.5) as well as very close eigenvalues (1% relative difference), which means an almost null slope on the DOS curve.
- The third slope breakdown appears for mode 25, linked to new central-part localised modes. The integrated DOS slope follows the same slope augmentation than for the first slope breakdown.
- Finally, mode 27 has a frequency almost equals to the non-overloaded beam mode 27 (about 1% of relative difference). Indeed, the overload distribution has almost no impact on mode shape because over masses are located on vibration nodes, which do not affect the dynamic behaviour.

If Figure 5 is then analysed, plotting integrated DOS of the 80 first modes, the behaviours previously identified

duplicate with frequency growth. So the pattern of the 27 first modes of Figure 4 is valid for the 27 following modes (from 28 to 54), so on and so forth (zones are identified on the curve by grey vertical dash lines).

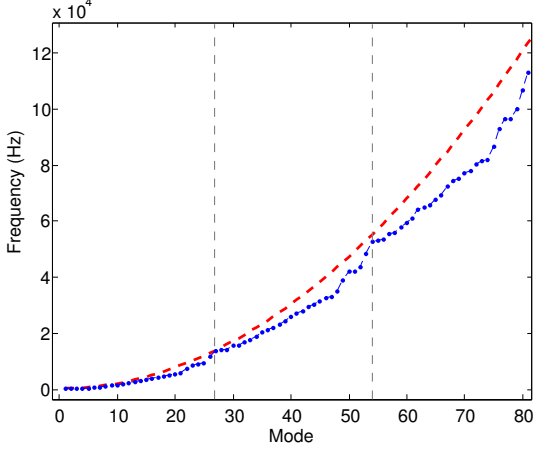


Figure 5: Natural frequencies of the first 80 modes : (---) classical beam, (---) pre-fractal beam (order 3), in linear scale.

Integrated DOS curves give information about the localised or extended nature of the mode, as well as the localisation type (central or lateral) of transverse displacement and about the overloading distribution. Here are all the elements of a periodic network coupled with a multi-scale distribution : this is the pre-fractal structure signature.

## 5 VIBROACOUSTIC COUPLING AND ACOUSTIC RADIATION

This part studies the modification of the acoustic response of a baffled structure, from the mechanical behaviour of the overloaded beam. Modes with a strong localisation of the transverse displacement presents an acoustic radiation attenuated in some frequencies regions.

### 5.1 Acoustic radiation modelling

As demonstrated by Elliott and Johnson,<sup>[16]</sup> total acoustic radiated power can be calculated either by mode amplitudes of the vibrating structure or from wall celerities from a network of elementary radiating elements.

Without full analytical formulation, the second way seems more relevant. Far-field acoustic radiated power can be evaluated from Radiation Resistance Matrix (abbreviated RRM). Assuming a time-harmonic motion, the vibrating surface is divided into  $N_{\text{rad}}$  rectangular elementary radiators, considered as monopoles vibrating at normal surface velocities of complex amplitudes

described in column vector  $\mathbf{v}_e$ . If the wall sound pressures acting on each grid element are also assembled into a column vector  $\mathbf{p}_e$ , the far-field total acoustic sound power  $P_{\text{ac}}(\omega)$  radiated by a baffled structure can be formulated as the summation of the radiated powers of each element, leading to Eq. (12)

$$P_{\text{ac}}(\omega) = \frac{S}{2N_{\text{rad}}} \Re\{\mathbf{v}_e^{\text{H}}(\omega) \cdot \mathbf{p}_e(\omega)\}, \quad (12)$$

where superscript  $\text{H}$  refers to the Hermitian transpose. Elementary radiator sizes have to be smaller than both structural and acoustic wavelengths (typically about the quart of them) and the structure is considered as baffled, under the classical hypotheses.<sup>[12,16]</sup> The size-to-frequency limitation might be approached as high order modes getting closer, but the acoustic efficiency tending to unity physically means that the modal critical frequency has been reached (which can be proved by an analytical study).

Sound pressure vector can be described by the complex impedance matrix relation as

$$\mathbf{p}_e(\omega) = [Z(\omega)] \mathbf{v}_e(\omega). \quad (13)$$

Then, the radiated resistance matrix  $[R] = \frac{S}{2N_{\text{rad}}} \Re[Z]$  can be written as Eq. (14)

$$[R(\omega)] = \frac{\omega^2 S^2 \epsilon \rho_0}{4\pi c_0} \begin{bmatrix} 1 & \frac{\sin(kr_{12})}{kr_{12}} & \dots & \frac{\sin(kr_{1N_x})}{kr_{1N_x}} \\ \frac{\sin(kr_{21})}{kr_{21}} & 1 & & \vdots \\ \vdots & & \ddots & \vdots \\ \frac{\sin(kr_{N_x 1})}{kr_{N_x 1}} & \dots & \dots & 1 \end{bmatrix} \quad (14)$$

to finally recast Eq. (12) into

$$P_{\text{ac}}(\omega) = \mathbf{v}_e^{\text{H}}(\omega) [R(\omega)] \mathbf{v}_e(\omega). \quad (15)$$

### 5.2 Acoustic modal efficiency simulation

Results are expressed as acoustic radiation efficiencies. Indeed, it is a more fundamental concept since it is independent from the absolute size of the radiating element and from the characteristic impedance of the propagation medium.<sup>[17]</sup> It is defined as

$$\sigma(\omega) = \frac{P_{\text{ac}}(\omega)}{P_{\text{vib}}(\omega)} = \frac{P_{\text{ac}}(\omega)}{\rho_0 c_0 S \langle v_n^2(\omega) \rangle}, \quad (16)$$

where  $\rho_0 c_0$  is the characteristic impedance of the air and  $P_{\text{vib}}$  the vibrational reference power generated by a piston uniformly vibrating with  $\langle v_n^2(\omega) \rangle$  the normal averaged quadratic surface velocity.

Figure 6 presents a simulation of acoustic radiation efficiency function of frequency of mode 26, for a non-overloaded beam and a pre-fractal beam of order 3, as well as mode 8 of a non-overloaded beam of length  $L_x/3$ . Here the results are presented in terms of modal acoustic efficiency, written  $\sigma_m$ , because it is taken for a given mode  $m$ .

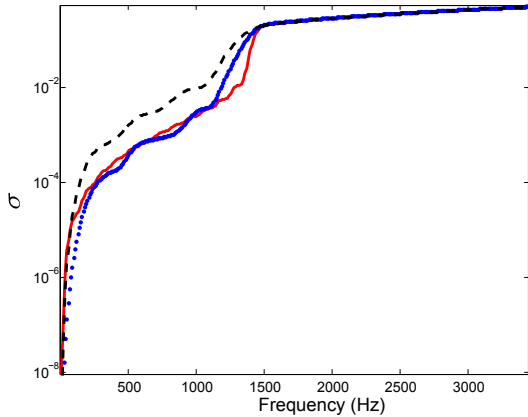


Figure 6: Acoustic radiation efficiency : mode 26 (—) classical beam, mode 26 (·) pre-fractal beam (order 3) and mode 8 (- -) of a non-overloaded beam of length  $L_x/3$ .

### 5.3 Analysis and discussion

Acoustic efficiency of a pre-fractal structure mode 26 is close to the mode 8 of a non-overloaded beam of length  $L_x/3$ , as plotted on Figure 6. Indeed, by comparing both mode shapes from Figure 3, the central part of the over-loaded beam can be identified as the principal vibrating zone and thus predominant in the acoustic radiation, which corresponds to the mode 8 of a non-overloaded beam of length  $L_x/3$ . It also corresponds to the central part of the Cantor set, of length a third of  $L_x$ . However, the efficiency of the self-similar beam is still slightly smaller, the lateral parts also contribute to reducing the global acoustic radiation.

Moreover, the frequencies of non-overloaded beam mode 8 and order 3 pre-fractal beam are similar (difference of about 5%) and so on for their modal critical frequencies. That reinforces the idea that these modes present some similarities in their acoustic radiation.

Finally, by comparing self-similar and non-overloaded beams of same length, the overloaded beam acoustic efficiency is slightly smaller in low frequencies. Efficiency then reaches the cross-over region and becomes larger until the modal critical frequency. The waviness of the non-overloaded beam is identified as side radiation lobes,<sup>[17]</sup> and it is even more tortuous as the mode is high-order. Yet, it is noticeable that the overloaded beam only presents a few, as the mode 8 of the beam of length  $L_x/3$ , which consolidates the idea that the acoustic radiation of the pre-fractal beam is driven by the central part of mode 8, where the transverse displacement has a larger amplitude (localised part).

## 6 CONCLUSION

This paper has presented the vibroacoustic model of a sandwich beam overloaded by a pre-fractal distribution of masses. The sandwich structure is modelled as a homogenised material under simple bending dynamics, then discretised and approximated by a finite difference method. Heterogeneities are integrated within the material such as additional masses distributed following a Canto-like set. The eigenvalue problem is then solved numerically to obtain the *in vacuo* modal basis.

Modal shapes have been presented for different orders. The chosen mode presents the localisation behaviour of the transverse displacement in the central part of the beam. The impact of the fractal order at iso local-overloading is then investigated at order 2 and 3, and a large localisation increase is identified by comparing maximal amplitudes of central and lateral parts.

Integrated DOS enables to feature localised modes through slope breakdowns as well as the type of localisation (central or lateral). The modes for which the over-masses are situated on vibration nodes are also identified because frequencies of non-overloaded and pre-fractal beams match as their mode shapes do.

Afterwards, fluid-structure coupling has been modelled through elementary radiators and the acoustic efficiency extracted from radiated acoustic power is calculated using a radiation resistance matrix. The acoustic radiation efficiency of the overloaded beam is close to the one of a one-third length beam (global behaviour, waviness and modal critical frequency), while remaining slightly smaller. The pre-fractal beam and its localised modes appear to present a smaller acoustic radiation compared to a non-overloaded beam in a given frequency range.

The interest of using such self-similar construction process is intrinsically linked to its definition. Indeed, the heterogeneity disposition goes further than a simple periodic distribution, by adding a homothetic ratio linked to the scheme order  $n_{\text{frac}}$ . This adds the repetition of slope breakdowns in the integrated DOS, as illustrated on Figure 5. Furthermore, the over-mass distribution presents a real physical sense, contrary to current reduction techniques, as viscoelastic patches for instance.

Finally, the masses are added within the honeycomb core, so within the structure, contrary to viscoelastic treatments that are glued to the external skins. Therefore, they have a direct action on the mechanical waves in the material, acting on the wave propagation with phenomena induced by the heterogeneities.

## ACKNOWLEDGEMENTS

This research has been supported jointly by the Midi-Pyrénées region and ONERA (The French Aerospace Lab).

## REFERENCES

- [1] Frank Simon, Simone Pautin, and Daniel Biron. Optimization of sandwich trim panels for reducing helicopter internal noise. *ERF 30 Marseille*, 2004.
- [2] Denys J. Mead. Plates with regular stiffening in acoustic media: Vibration and radiation. *The Journal of the Acoustical Society of America*, 88(1): 391–401, 1990.
- [3] Denys J. Mead. Wave propagation in continuous periodic structures : Research contributions from Southampton, 1964-1995. *Journal of Sound and Vibration*, 190(3):495–524, 1996.
- [4] R. S. Langley. Wave transmission through one-dimensional near periodic structures: optimum and random disorder. *Journal of Sound and Vibration*, 188(5):717–743, 1995.
- [5] S. Alexander and R. Orbach. Density of states on fractals : “fractons”. *Journal de Physique - Lettres*, 43(17):625–631, 1982.
- [6] Etienne Bertaud du Chazaud and Vincent Gibiat. A numerical study of 1D self-similar waveguides: Relationship between localization, integrated density of state and the distribution of scatterers. *Journal of Sound and Vibration*, 313(3-5):631–642, 2008.
- [7] Etienne Bertaud du Chazaud, Delphine Chareyron, and Vincent Gibiat. Elastic waves in 2D self-similar structures : localisation, vibrational integrated density of state and distribution of the scatterers. *Forum Acusticum Budapest*, 2005.
- [8] Djamel Bouzit and Christophe Pierre. Localization of vibration in disordered multi-span beams with damping. *Journal of Sound and Vibration*, 187(4): 625–648, 1995.
- [9] Djamel Bouzit and Christophe Pierre. An experimental investigation of vibration localization in disordered multi-span beams. *Journal of Sound and Vibration*, 187(4):649–669, 1995.
- [10] ONERA/ATECA. Panneau insonorisant, Brevet INPI 3017235. Bulletin 32 du 7 Août, 2015.
- [11] D. Backström and Anders C. Nilsson. Modelling the vibration of sandwich beams using frequency-dependent parameters. *Journal of Sound and Vibration*, 300:589–611, 2007.
- [12] Frank Fahy and Paolo Gardonio. *Sound and structural vibration - Radiation, transmission and response*. Academic Press, Elsevier, second edition, 2007.
- [13] Anders C. Nilsson. Wave propagation in and sound transmission through sandwich plates. *Journal of Sound and Vibration*, 138(1):73–94, 1990.
- [14] Hyeung-Yun Kim and Woonbong Hwang. Effect of debonding on natural frequencies and frequency response functions of honeycomb sandwich beams. *Composite Structures*, 55(1):51–62, January 2002.
- [15] K. B. Subrahmanyam and A. W. Leissa. An improved finite difference analysis of uncoupled vibrations of cantilevered beams. *Journal of Sound and Vibration*, 98(1):1–11, 1985.
- [16] S. J. Elliott and M. E. Johnson. Radiation modes and the active control of sound power. *Journal of the Acoustical Society of America*, 94(4):2194–2204, 1994.
- [17] C. E. Wallace. Radiation resistance of a baffled beam. *The Journal of the Acoustical Society of America*, 51(3):936–945, 1972.

## APPENDIX

Quantity		
Designation	Unit	Value
$L_x$	(m)	1
$L_y$	(m)	0.05
$h$	(m)	0.0104
$\rho$	(kg.m <sup>-3</sup> )	264.4
$D$	(Pa.m <sup>4</sup> )	19.8
$N$		243
$\alpha_{loc}$		0.071

Table 1: Quantities and values of numerical simulations.